Hindawi
Journal of Nanomaterials
Volume 2022, Article ID 2650421, 13 pages
https://doi.org/10.1155/2022/2650421

Research Article

Hydrogenated TiO_2 Nanotubes Regulate Osseointegration by Influencing Macrophage Polarization in the Osteogenic Environment

Xu Cao, Ran Lu, Xin Wang, Caiyun Wang, Yu Zhao, Yuchen Sun, and Su Chen

Laboratory of Biomaterials and Biomechanics, Beijing Key Laboratory of Tooth Regeneration and Function Reconstruction, Beijing Stomatological Hospital, Capital Medical University, Beijing, China

Correspondence should be addressed to Su Chen; chensu@mail.ccmu.edu.cn

Received 5 July 2022; Revised 24 October 2022; Accepted 28 October 2022; Published 29 December 2022

Academic Editor: Ruibing Wang

The immunomodulatory role of monocytes is essential for tissue healing and can influence the osseointegration of implanted materials. Properties such as the surface structure, hydrophilicity, and roughness of the implanted materials can modulate monocyte–macrophage function. In this study, we characterized material-hydrogenated TiO_2 nanotubes (H-TNT) with superhydrophilic surfaces to investigate the effect of H-TNT on macrophage polarization and osseointegration. H-TNT were prepared by anodic oxidation and hydrogenation and used in the experimental group, while TNT and smooth pure Ti were employed in the control groups. RAW264.7 cells were selected to observe the immunomodulatory effect of these samples. The cell morphology was observed via scanning electron microscopy, and cytokine expression was detected using an enzyme-linked immunosorbent assay and immunofluorescence staining. After 24 hr of cultivation, the macrophage-conditioned medium was collected and used for indirect coculture with MC3T3-E1 cells. The morphology of MC3T3-E1 cells was observed using fluorescence staining. Cell adhesion and proliferation were measured using the Cell Counting Kit-8 assay. Alkaline phosphatase activity measurement, alizarin red staining, calcium quantification, and reverse transcription polymerase chain reaction were performed to assess the osteogenic differentiation of MC3T3-E1 cells. The results showed that H-TNT promoted the M2-type polarization of macrophages, which in turn influenced the adhesion, proliferation, and osteogenic differentiation of MC3T3-E1 cells. These materials can serve as useful candidates for bone implants because they activate macrophages to produce a favorable osteoimmunomodulatory microenvironment.

1. Introduction

Optimal osseointegration is critical for successful implantation. Activation of the immune response greatly affects the long-term survival of dental implants [1]. Following implantation, activation of the inflammatory response is the initial and most important event [2]. The healing process is accompanied by a series of immunomodulatory responses. As the primary upstream inflammation regulators, macrophages play a key role in the recognition and destruction of foreign materials and are involved in the secretion of cytokines, chemokines, and growth factors that determine inflammation onset and subsequent tissue healing. In addition, they greatly influence bone formation and remodeling [3, 4]. As macrophages exert significant effects on tissue repair, their immunomodulatory effect is crucial for evaluating implanted materials.

Macrophages possess remarkable plasticity. Based on the microenvironment, they can differentiate into M1 macrophages, which promote inflammation by increasing the expression of proinflammatory cytokines such as interleukin (IL)-6 (IL-6) and tumor necrosis factor-α (TNF-α) [5]; they can also differentiate into M2 macrophages, which reduce inflammation and promote tissue healing by increasing the expression of anti-inflammatory cytokines such as IL-4, IL-10, and arginase 1 [6–10]. This process, termed macrophage polarization, governs the biological performance of biomaterials and wound healing [11, 12].

A previous study demonstrated that material surface properties, such as nanotopography, hydrophilicity, and roughness, affect macrophage polarization [13], which in turn can regulate bone formation [14–17]. Nanotopography downregulated the expression of the proinflammatory cytokine TNF-α, which remained detectable after 21 days. Furthermore, the nanotopography attenuated the initial inflammatory response and promoted bone formation, while downregulating osteoclastogenesis and bone resorption molecules [18]. Additionally, hydrophilic Ti surface can regulate the expression of inflammation-related factors in macrophages and reduce inflammation. Studies have shown that smooth surface Ti induces M1-type polarization of macrophages, resulting in a significant increase of IL-1β, IL-6, and TNF-α expression; in contrast, hydrophilic rough surface Ti induces M2-type polarization of macrophages, resulting in a significant increase in IL-4 and IL-10 expression [13]. Thus, an increase in hydrophilicity and roughness can induce macrophages to undergo M2-type polarization and generate an anti-inflammatory microenvironment that promotes osseointegration.

Increasing evidence indicates that TiO_2 nanotubes (TNT) can induce macrophage polarization owing to their nanomorphology, thereby promoting bone formation. Nanotubes within a narrow size range (70–80 nm) reduce the expression of TNF-α, IL-1β, monocyte chemoattractant protein 1, IL-6, and macrophage inflammatory protein 1 α in primary human monocytes and macrophages as well as macrophage cell lines [19, 20]. Compared with other nanoparticles, such as nanopore and nanopit, the nanotubes produced by anodization are uniform, exhibit a regular morphology, and have tunable lengths and diameters [21]. In addition, nanotube arrays mimic the size and arrangement of collagen fibrils in bone tissue [22], favoring osteogenesis. Furthermore, the spacing of the nanotubes facilitates nutrient availability and waste removal [23]. Based on this information, we prepared uniformly arranged TNT arrays of ~100 nm diameters by anodization and further increased the TNT hydrophilicity via hydrogenation treatment. Hydrogenated TNT (H-TNT) exhibit nanomorphology, superhydrophilicity, and excellent protein adsorption [24] and may induce M2-type macrophage polarization [25]. The present study investigated whether superhydrophilic H-TNT can regulate M2-type macrophage polarization, thereby promoting the osteogenic differentiation of osteoblasts and accelerating osseointegration after implantation.

2. Materials and Methods

2.1. Ti, TiO_2 Nanotube, and Hydrogenated TiO_2 Nanotube Fabrication. TNT were prepared using the methodology of Lu et al. [24]. The smooth pure Ti substrates (1 cm × 1 cm) were ultrasonically cleaned in acetone, ethanol, and deionized water for 10 min. The samples were then anodized for 15 min at 50 V in an ethylene glycol electrolyte (containing 0.5 wt% ammonium fluoride and 10 vol% deionized water) to fabricate TNT to be used in the control group. After the anodization and hydrogenation processes, H-TNT were produced to be used in the experimental group, while the smooth pure Ti substrates served as a blank control (Ti) group.

2.2. Sample Characterization. The surface morphologies and chemical states of the samples were observed using scanning electron microscopy (SEM; S4800, Hitachi Ltd., Japan) and X-ray photoelectron spectroscopy (XPS; ESCALAB 250Xi, Thermo Fisher Scientific, USA), respectively. The water contact angles (CAs) were measured using a contact analysis system (Model OCA15pro, Dataphysics Co., Ltd., Germany). The sample roughness was analyzed using atomic force microscopy (AFM; Nanoscope V, Veeco Instrument Inc., USA).

2.3. Cell Culture. RAW 264.7 and MC3T3-E1 cells (China Infrastructure of Cell Line Resource, China) were cultured under standard culture conditions to evaluate their immunomodulatory effects and osteogenic differentiation.

2.4. Macrophage Morphology. RAW 264.7 cells were seeded on Ti, TNT, and H-TNT surfaces. After culturing for 24 hr, the cells were rinsed, fixed, dehydrated, dried, and subjected to gold coating. Their morphology was then observed using SEM.

2.5. Cytokine Analysis. RAW 264.7 cells were seeded on Ti, TNT, and H-TNT surfaces and incubated for 24 hr. The concentrations of TNF-α, IL-6, IL-4, and IL-10 in the supernatant were determined using an enzyme-linked immunosorbent assay kit (Abclonal, China).

2.6. Cytoimmunofluorescence of Macrophage Polarization-Related Proteins. RAW 264.7 cells were seeded on Ti, TNT, and H-TNT surfaces. After incubation for 24 and 48 hr, adherent RAW 264.7 cells were washed twice with phosphate-buffered saline (PBS) and fixed with 4% paraformaldehyde at room temperature for 15 min. The samples were gently washed three times with PBS and blocked with 10% goat serum. The pro- and anti-inflammatory biomarkers iNOS (Abclonal, China) and CD80 (Abclonal, China), respectively, were labeled green, and the nuclei were stained with 4′,6-diamidino-2-phenylindole (DAPI) (ZSGB-BIO, China).

2.7. Preparation of Macrophage-Conditioned Medium. RAW 264.7 cells were seeded on the sample surfaces. After 24 hr of cultivation [10], the Ti, TNT, and H-TNT supernatants were harvested, centrifuged, and diluted with complete Dulbecco's modified eagle medium in a ratio of 1 : 1 to produce macrophage-conditioned media (MCM) composed of Ti, TNT, and H-TNT. Subsequently, the MCM was used for indirect cocultivation.

2.8. Cytoimmunofluorescence of MC3T3-E1 Cells. MC3T3-E1 cells were seeded on glass coverslips in 24-well plates and indirectly cocultured with the Ti, TNT, and H-TNT MCM after 24 hr. After indirect coculture for 1, 2, or 3 days, the MC3T3-E1 cells were fixed with 4% paraformaldehyde, permeabilized with 0.1% Triton X-100, and blocked with 10% goat serum. Alexa Fluor 594 phalloidin (Cell Signaling

Table 1: Primers used in real-time RT-PCR.

Gene	Forward primer sequence (5′–3′)	Reverse primer sequence (5′–3′)
BMP-2	GGGACCCGCTGTCTTCTAGT	TCAACTCAAATTCGCTGAGGAC
Runx2	ATGCTTCATTCGCCTCACAAA	GCACTCACTGACTCGGTTGG
OPN	GTGATTTGCTTTTGCCTGTTTG	GGAGATTCTGCTTCTGAGATGGG
OCN	GAACAGACAAGTCCCACACAGC	TCAGCAGAGTGAGCAGAAAGAT
ALP	GAACAGAACTGATGTGGAATACGAA	CAGTGCGGTTCCAGACATAGTG
COL-1	GATGTTGAACTTGTTGTTGCTGAGGG	GGCAGGCGAGATGGCTTATT
GAPDH	TGTGTCCGTCGTGGATCTGA	TTGCTGTTGAAGTCGCAGGAG

Technology, USA) was used to fluorescently label the actin cytoskeleton. The cell nuclei were stained with DAPI.

2.9. Cell Adhesion and Proliferation. MC3T3-E1 cells were seeded in blank 96-well plates (2×10^4 cells/cm^2) and incubated with the Ti, TNT, or H-TNT MCM. For the adhesion and proliferation assays, the cells were incubated for 1, 2, or 4 hr and 1, 3, 5, or 7 days, respectively. The Cell Counting Kit-8 (CCK-8, Japan) was used according to the manufacturer's instructions for both the adhesion and proliferation assays.

2.10. Alkaline Phosphatase Activity. MC3T3-E1 cells were seeded in blank 24-well plates (2×10^4 cells/cm^2). After indirect coculture with an MCM and osteogenic induction for 3, 5, or 7 days, adherent MC3T3-E1 cells were lysed in a radioimmunoprecipitation assay solution. The alkaline phosphatase (ALP) activity was determined using an ALP assay kit (Beyotime, China), according to the manufacturer's instructions. A bovine serum albumin kit (Sigma-Aldrich, St. Louis, USA) was used according to the manufacturer's instructions to normalize the ALP activity.

2.11. Quantification of Mineralization. MC3T3-E1 cells were seeded in blank 6-well plates (2.5×10^4 cells/cm^2). After 14 and 21 days of indirect coculture and osteogenesis induction, the cells were fixed with 95% ethanol and incubated with 40 mM Alizarin Red S (pH 4.2, Sigma-Aldrich, USA) for 30 min [26]. After extensive washing with distilled water, the calcium nodule formation was observed using a stereomicroscope (Leica, Germany). To determine the calcium ion concentration, 1 ml of 10% cetyl pyridinium chloride solution was added to each well, and the absorbance was subsequently measured at 570 nm using a spectrophotometer (SpectraMax Paradigm, USA).

2.12. Quantitative Reverse Transcription Polymerase Chain Reaction. MC3T3-E1 cells were seeded in 6-well culture plates (2.5×10^4 cells/cm^2). After indirect cocultivation with an MCM and osteogenic induction for 3 days, RNA was extracted from MC3T3-E1 cells using the TRIzol reagent (Invitrogen, USA) and reverse-transcribed to cDNA (Takara, Japan). A reverse transcription polymerase chain reaction was used to detect bone morphogenetic protein 2 (BMP-2), Runx2, osteopontin (OPN), osteocalcin (OCN), ALP, collagen type 1 (COL-1), and glyceraldehyde 3-phosphate dehydrogenase (GAPDH) expression. The sequences of primers used are listed in Table 1.

2.13. Statistical Analysis. All data are presented as the mean ± standard deviation. The data were analyzed using one-way analysis of variance with SPSS 20.0 software (IBM Corp., USA). The statistical significance was set at $p < 0.05$.

3. Results and Discussion

3.1. Sample Characterization. The SEM images showed comparable surface morphologies for TNT and H-TNT (Figure 1(a)). The nanotubes were well-organized, with diameters of ~100 nm. The Ti substrates displayed the highest water CA of 90.95°, followed by 46.98° for TNT and 5.25° for H-TNT, which were super hydrophilic (Figures 1(b) and 1(c)). The surface roughness values of the three samples were characterized using AFM, as shown in Figure 1(d). The TNT and H-TNT samples exhibited higher roughness than Ti owing to nanotube array formation; however, the TNT and H-TNT samples showed no significant changes. The chemical compositions and oxidation states of the TNT and H-TNT samples were investigated using XPS, as shown in Figure 1(e). Peaks corresponding to Ti–O–Ti (529.9–530.4 eV) and Ti–OH (532.0 eV) appeared in the TNT and H-TNT spectra. Notably, the Ti–OH peak intensity of the H-TNT sample was significantly higher than that of the TNT sample, suggesting that after hydrogenation, the TNT surface was functionalized by hydroxyl groups, increasing the sample wettability. The X-ray diffraction patterns of the samples demonstrated that the basic crystal structure did not change after hydrogenation (Figure 1(f)). Compared with that of the TNT sample, the anatase peak intensity of the H-TNT sample was slightly weakened, indicating the presence of oxygen vacancies in the TiO lattice due to hydrogenation [27].

3.2. Inflammatory Responses of Macrophages

3.2.1. Field-Emission Scanning Electron Microscopy Images. After culturing RAW264.7 cells for 4 and 24 hr, the cell morphology was assessed using field-emission SEM. As shown in Figure 2, the macrophages grown on Ti displayed a spread-out morphology, whereas those cultured on TNT and H-TNT had a round morphology.

3.2.2. Cytokine Secretion from RAW264.7 Cells. The levels of the proinflammatory cytokines TNF-α and IL-6 in the Ti and TNT samples were significantly higher than those in the H-TNT sample (Figures 3(a) and 3(b)). In contrast, the levels of the anti-inflammatory cytokines IL-4 and IL-10 in the H-TNT sample were considerably higher than those in

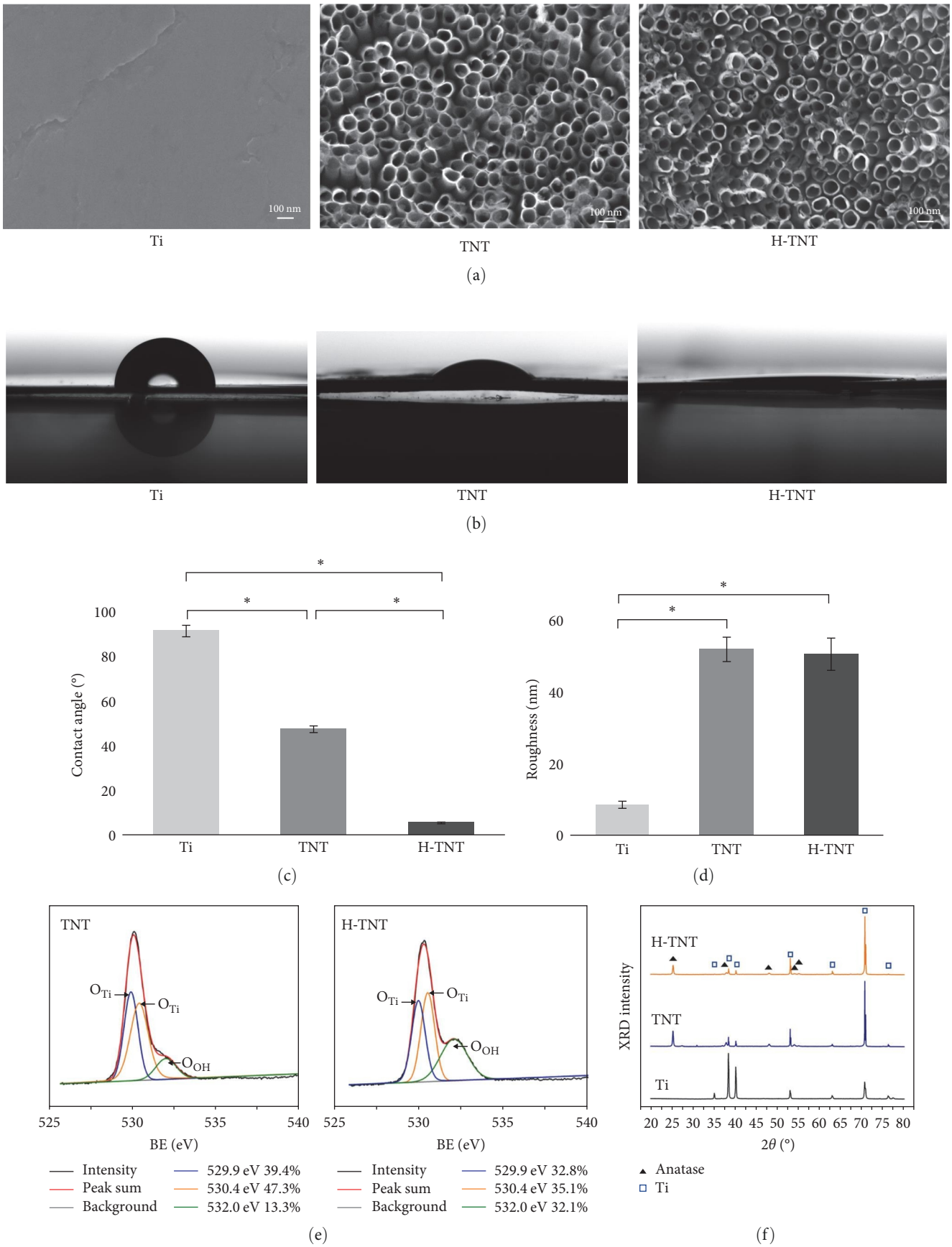

Figure 1: (a) SEM images of TNT and H-TNT samples; (b) water CA values of Ti, TNT, H-TNT; (c) histogram of water contact angle; (d) histogram of roughness; (e) high-resolution XPS spectra of O 1s; (f) XRD patterns of Ti substrate, TNT, and H-TNT. Abbreviations: H-TNT, hydrogenated TiO_2 nanotubes; Ti, pure titanium; TNT, air-annealed TiO_2 nanotubes; XPS, X-ray photoelectron spectroscopy. XRD, X-ray diffraction. $^*p < 0.05$.

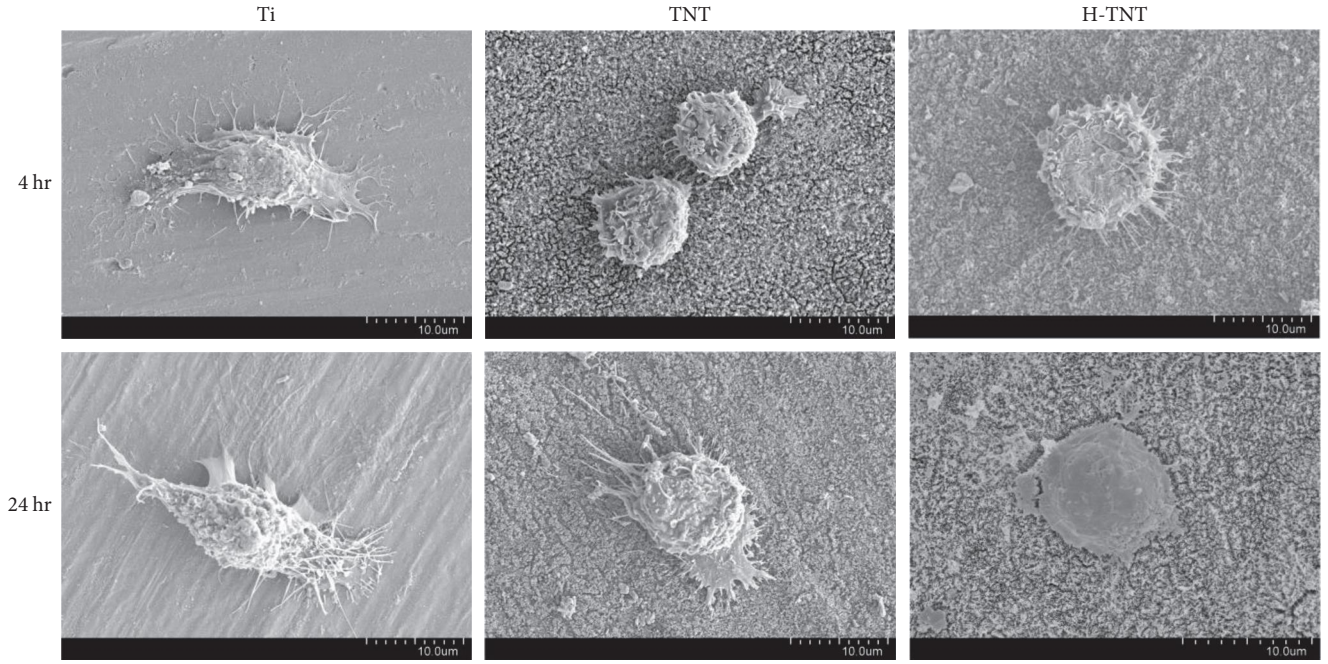

Figure 2: Scanning electron microscopy (SEM) images of RAW264.7 cell morphology. Abbreviations: H-TNT, hydrogenated TiO_2 nanotubes; Ti, pure titanium; TNT, air-annealed TiO_2 nanotubes.

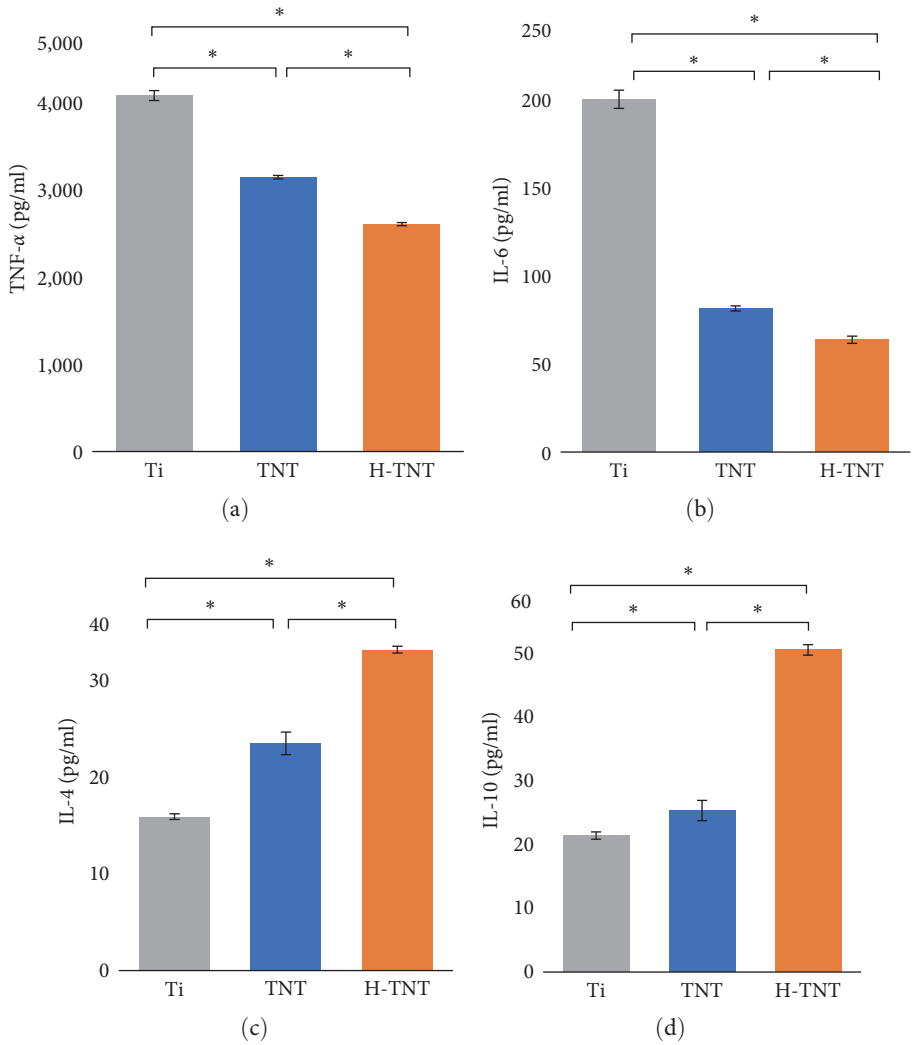

Figure 3: Pro- and anti-inflammatory cytokine levels at 24 hr: (a) TNF-α; (b) IL-6; (c) IL-4; and (d) IL-10. $^*p < 0.05$. Abbreviations: H-TNT, hydrogenated TiO_2 nanotubes; IL, interleukin; Ti, pure titanium; TNF-α, tumor necrosis factor α; TNT, air-annealed TiO_2 nanotubes.

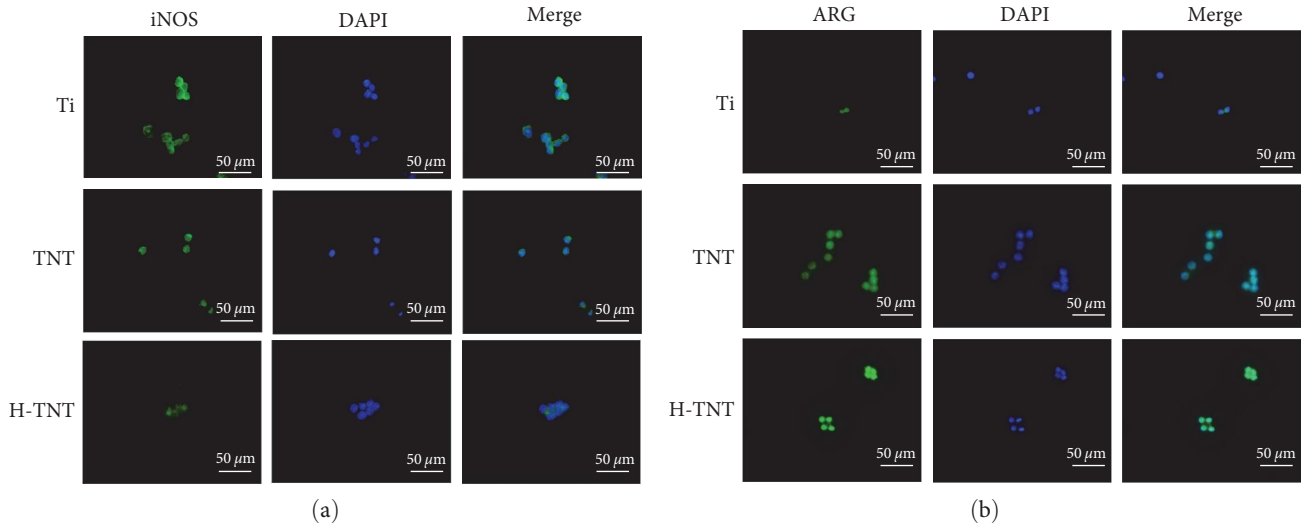

Figure 4: Immunofluorescent staining of macrophages at 24 hr: (a) iNOS was labeled green and nuclei were stained with DAPI; (b) ARG was labeled green, and nuclei were stained with DAPI; "Merge" represents the merged images of iNOS or ARG and nuclei. Abbreviations: DAPI, 4′,6-diamidino-2-phenylindole; H-TNT, hydrogenated TiO_2 nanotubes; Ti, pure titanium; TNT, air-annealed TiO_2 nanotubes.

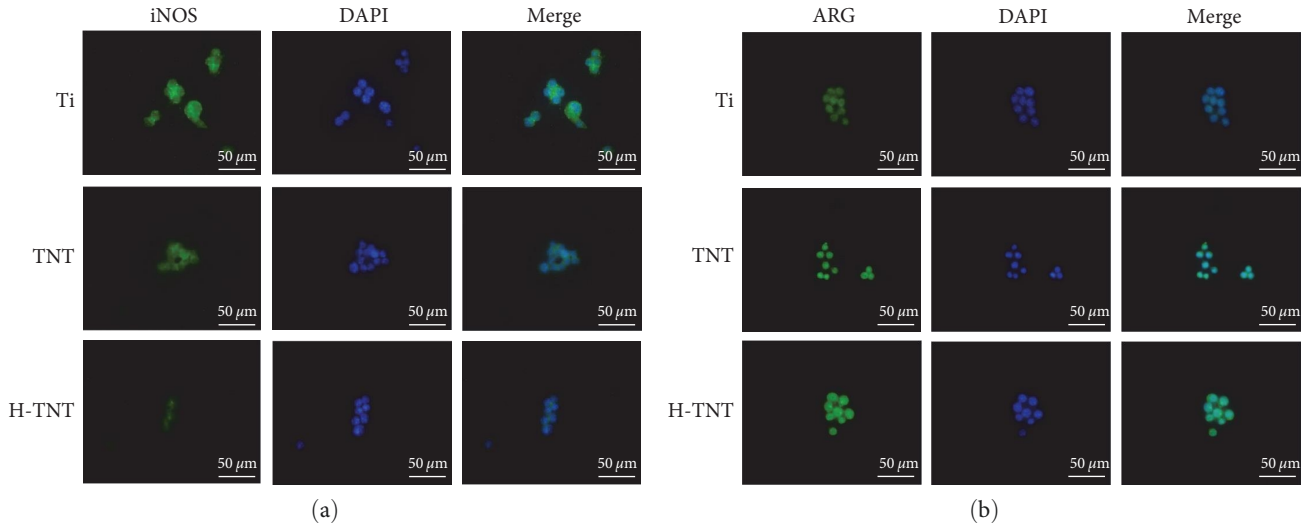

Figure 5: Immunofluorescent staining of macrophages at 48 hr: (a) iNOS was labeled green and nuclei were stained with DAPI; (b) ARG was labeled green, and nuclei were stained with DAPI; "Merge" represents the merged images of iNOS or ARG and nuclei. Abbreviations: DAPI, 4′,6-diamidino-2-phenylindole; H-TNT, hydrogenated TiO_2 nanotubes; Ti, pure titanium; TNT, air-annealed TiO_2 nanotubes.

the Ti and TNT samples (Figures 3(c) and 3(d)). Furthermore, the differences among the three samples were statistically significant ($p < 0.05$).

3.2.3. Immunofluorescent Staining of Macrophages. The macrophages grown on Ti showed the maximum expression of iNOS, a proinflammatory marker (Figures 4(a) and 5(a)), whereas the macrophages grown on H-TNT and TNT expressed the maximum levels of ARG, an anti-inflammatory marker (Figures 4(b) and 5(b)). To further confirm macrophage polarization, immunofluorescence staining for CD80 and CD163 was performed. The results showed that the macrophages grown on Ti expressed the highest levels of the CD80, a proinflammatory marker of M1 macrophages (Figures 6(a) and 7(a)), and displayed a stretched, spindled morphology (Figure 6(a)). More cell samples can be found in the supplementary Figures S1, S2, and S3. In contrast, the macrophages grown on H-TNT expressed the highest levels of CD163, an anti-inflammatory marker of M2 macrophages, and displayed a rounded morphology (Figures 6(b) and 7(b)), consistent with the results of fluorescence staining quantitative analysis (supplementary Figures S4, S5, S6, and S7).

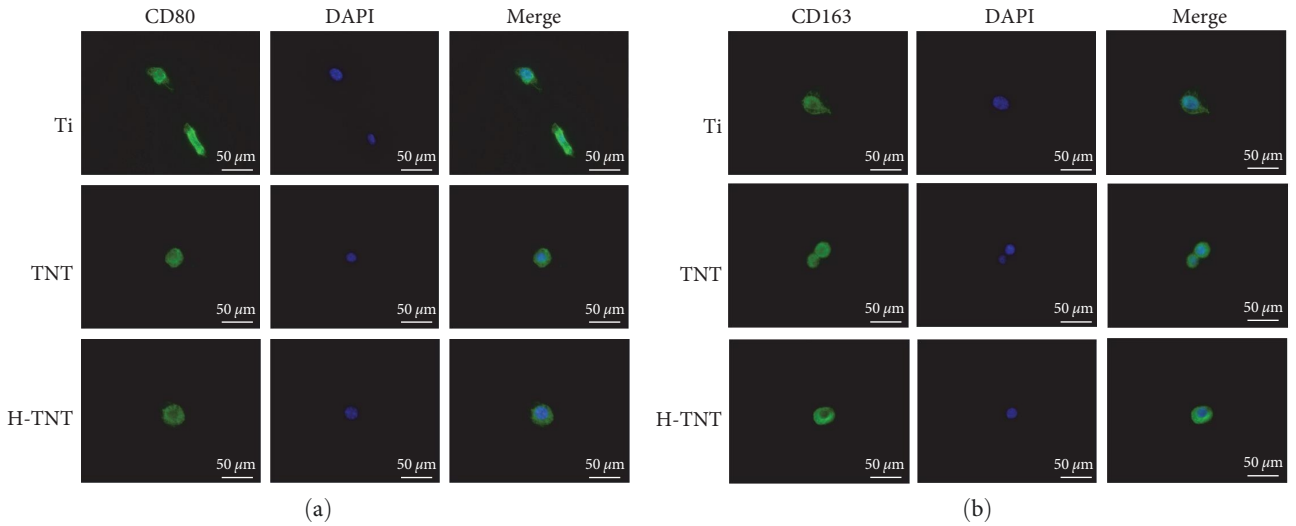

Figure 6: Immunofluorescent staining of macrophages at 24 hr: (a) CD80 was labeled green and nuclei were stained with DAPI; (b) CD163 was labeled green, and nuclei were stained with DAPI. "Merge" represents the merged images of CD80 or CD163 and nuclei. Abbreviations: DAPI, 4′,6-diamidino-2-phenylindole; H-TNT, hydrogenated TiO_2 nanotubes; Ti, pure titanium; TNT, air-annealed TiO_2 nanotubes.

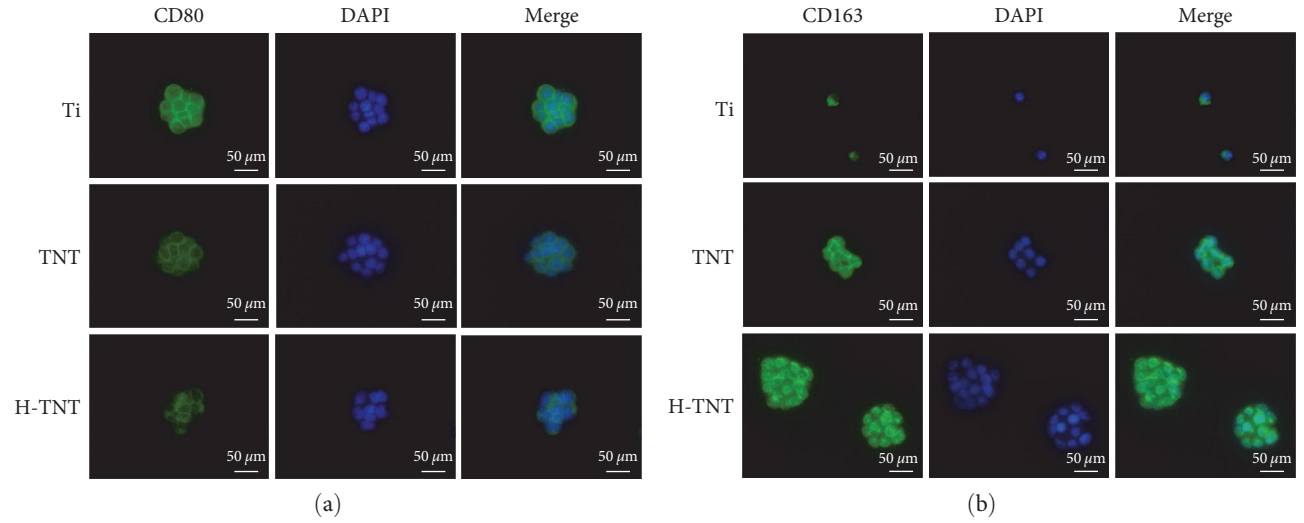

Figure 7: Immunofluorescent staining of macrophages at 48 hr: (a) CD80 was labeled green and nuclei were stained by DAPI; (b) CD163 was labeled green and nuclei were stained by DAPI. "Merge" represented the merged images of CD80 or CD163 and nuclei. Abbreviations: DAPI, 4′,6-diamidino-2-phenylindole; H-TNT, hydrogenated TiO_2 nanotubes; Ti, pure titanium; TNT, air-annealed TiO_2 nanotubes.

3.3. Macrophages on Hydrogenated TiO_2 Nanotube Arrays Enhance Osteogenic Conditions

3.3.1. Effect of a Macrophage-Conditioned Medium on MC3T3-E1 Cell Morphology. Considering the modulatory effects of macrophage polarization on osteoblast behavior, we performed an indirect coculture of MC3T3-E1 and RAW264.7 cells. The MC3T3-E1 cells were treated with Ti, TNT, and H-TNT MCM for 1, 2, and 3 days, respectively. The fluorescence microscopy images (Figure 8) show that MC3T3-E1 cells of the Ti sample were polygonal in shape. Compared with cells cultivated in the TNT and Ti MCM, the cells cultivated in the H-TNT MCM were more elongated and displayed extended cytoskeletons on days 2 and 3.

3.3.2. Effect of a Macrophage-Conditioned Medium on MC3T3-E1 Cell Adhesion and Proliferation. Cell adhesion with the H-TNT MCM was significantly higher than that with the Ti MCM after 1, 2, and 4 hr of incubation (Figure 9) and higher than that with the TNT MCM after 2 hr. Moreover, the cell proliferation activity in each sample gradually increased with time. With the H-TNT MCM, proliferation is the highest at all four time points ($p < 0.05$), indicating that the H-TNT MCM promotes the proliferation potential of MC3T3-E1 cells.

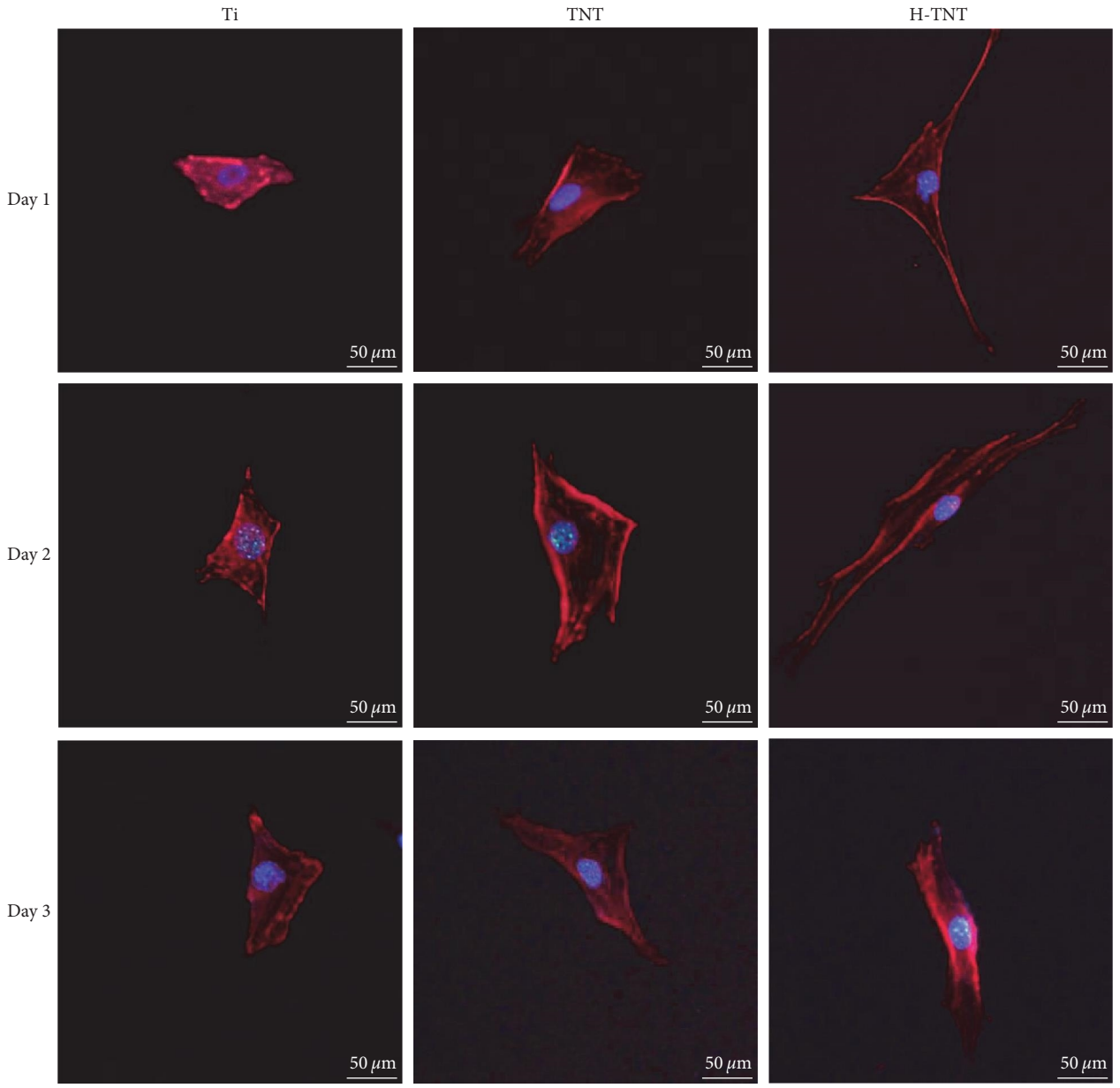

Figure 8: MC3T3-E1 cell morphology after culture with MCM for 1, 2, and 3 days. Abbreviations: H-TNT, hydrogenated TiO_2 nanotubes; MCM, macrophage-conditioned media; Ti, pure titanium; TNT, air-annealed TiO_2 nanotubes.

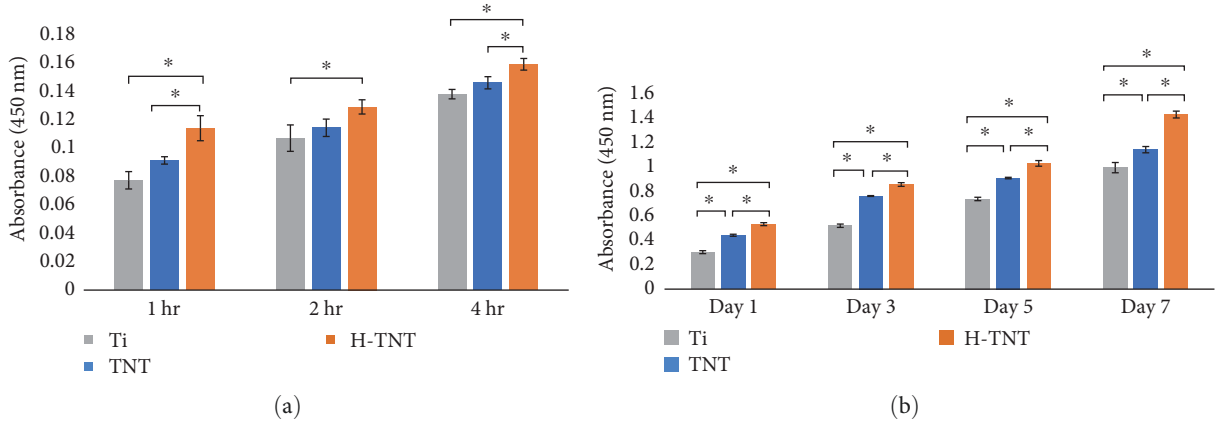

Figure 9: (a) CCK-8 results of MC3T3-E1 cell adhesion on samples after 1, 2, and 4 hr; (b) CCK-8 results of MC3T3-E1 cell proliferation on samples after 1, 3, 5, and 7 days. $^*p < 0.05$. Abbreviations: CCK-8, cell counting kit-8; H-TNT, hydrogenated TiO_2 nanotubes; Ti, pure titanium; TNT, air-annealed TiO_2 nanotubes.

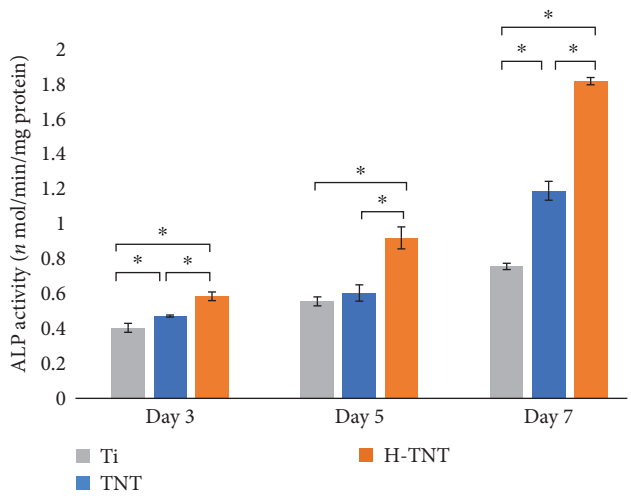

FIGURE 10: ALP activity of MC3T3-E1 cells after osteogenic induction for 3, 5, and 7 days. $^*p < 0.05$. Abbreviations: ALP, alkaline phosphatase; H-TNT, hydrogenated TiO_2 nanotubes; Ti, pure titanium; TNT, air-annealed TiO_2 nanotubes.

3.3.3. Effects of a Macrophage-Conditioned Medium on Alkaline Phosphatase Activity in MC3T3-E1 Cells. MC3T3-E1 cells were supplemented with an MCM harvested from RAW264.7 cultures grown on the Ti, TNT, and H-TNT surfaces. Maximum ALP activity was observed in the H-TNT sample on each day (Figure 10).

3.3.4. Effects of a Macrophage-Conditioned Medium on Mineralization in MC3T3-E1 Cells. After 14 and 21 days of indirect coculture and osteogenic induction, alizarin red *S* staining was used to detect the cell mineralization abilities of the samples (Figure 11(a)). Although calcium nodules could be observed in the H-TNT sample after 14 days, none appeared in the other two samples. After 21 days, the TNT sample contained more calcium nodules than the Ti sample, and the H-TNT sample displayed maximum extracellular matrix mineralization.

Quantitative analysis was performed after dissolving the calcium nodules in 10% cetyl pyridinium chloride (Figure 11(b)). After 14 days, maximum extracellular matrix mineralization was observed in the H-TNT sample. Additionally, the results obtained from the three samples after 21 days were statistically different ($p < 0.05$). Finally, the H-TNT sample exhibited the highest absorbance, followed by the TNT sample.

3.3.5. Effect of a Macrophage-Conditioned Medium on Osteogenic Gene Expression in MC3T3-E1 Cells. The mRNA levels of osteogenic genes were measured after 3 days of indirect cocultivation and osteogenic induction (Figure 12). As shown, the highest Runx-2, BMP-2, OPN, ALP, and COL-1 expression levels were observed in the H-TNT sample. Furthermore, BMP-2 mRNA levels considerably differed among the three samples ($p < 0.05$).

4. Discussion

In this study, we investigated the effect of H-TNT on macrophage activation and their paracrine interactions using MC3T3-E1 cells. H-TNT were capable of manipulating macrophage polarization, indicating that they could support osseointegration at the bone–material interface.

As the first cells to reach the implant interface, macrophages are regulated by the material surface characteristics, such as morphology, roughness, and hydrophilicity [13, 28, 29]. This suggests that they also affect osteogenesis, which is essential for implant survival. M1 macrophages express IL-6 and TNF-α, which delay bone healing and cause pathogenic bone loss. Conversely, M2 macrophages express IL-4 and IL-10, which reduce inflammation and promote wound healing [9, 30]. The polarization state of macrophages can be determined by detecting surface markers and secreted cytokines and chemokines.

The cells cultured with H-TNT secreted lower levels of IL-6 and TNF-α (proinflammatory factors) and higher levels of IL-4 and IL-10 (anti-inflammatory factors) than those cultured with Ti and TNT. Furthermore, the nanotubular topography and superhydrophilic properties of H-TNT may have promoted M2-type macrophage polarization. Studies have shown that nanotubes with a diameter of 100 nm provide more protein adsorption sites, as the gaps between the nanotubes serve as nutrient supply pathways [20, 31]. In addition, the TNT structure can inhibit inflammation [32]. Moreover, hydrophilic biomaterial surfaces can enhance macrophage apoptosis, increase anti-inflammatory cytokine secretion, and decrease proinflammatory factor levels [33, 34]. With an increase in the roughness and hydrophilicity of the biomaterial surface, macrophages may interact with adsorbed proteins to promote M2-type macrophage polarization. Our results are consistent with those of previous studies on the relationship between macrophage morphology and polarization status. A stretched morphology indicates cell activation and acquisition of migratory ability, whereas a round shape indicates that the cells are not activated [25, 35]. Hence, H-TNT with superhydrophilic nanotubular surfaces can promote macrophage activation to inhibit inflammation, reduce the inflammatory response of macrophages, and promote M2-type macrophage polarization for bone formation and tissue repair [36, 37].

An appropriate implant microenvironment is critical for successful osseointegration. However, it is inadequate to analyze macrophage polarization on the implant surface. Studying the effect of macrophages on osteoblasts can reveal the effect of immune regulation on osteogenic performance. MC3T3-E1 cells used in this study have good osteogenic differentiation potential. Therefore, they typically serve as an in vitro research model for osteoblast proliferation and mineralization [38]. Considering the super hydrophilicity and good protein adsorption of H-TNT, as well as their immunomodulatory effect on macrophage polarization, indirect RAW264.7 coculture was performed to explore the effects of M2 macrophages and H-TNT on MC3T3-E1 cells.

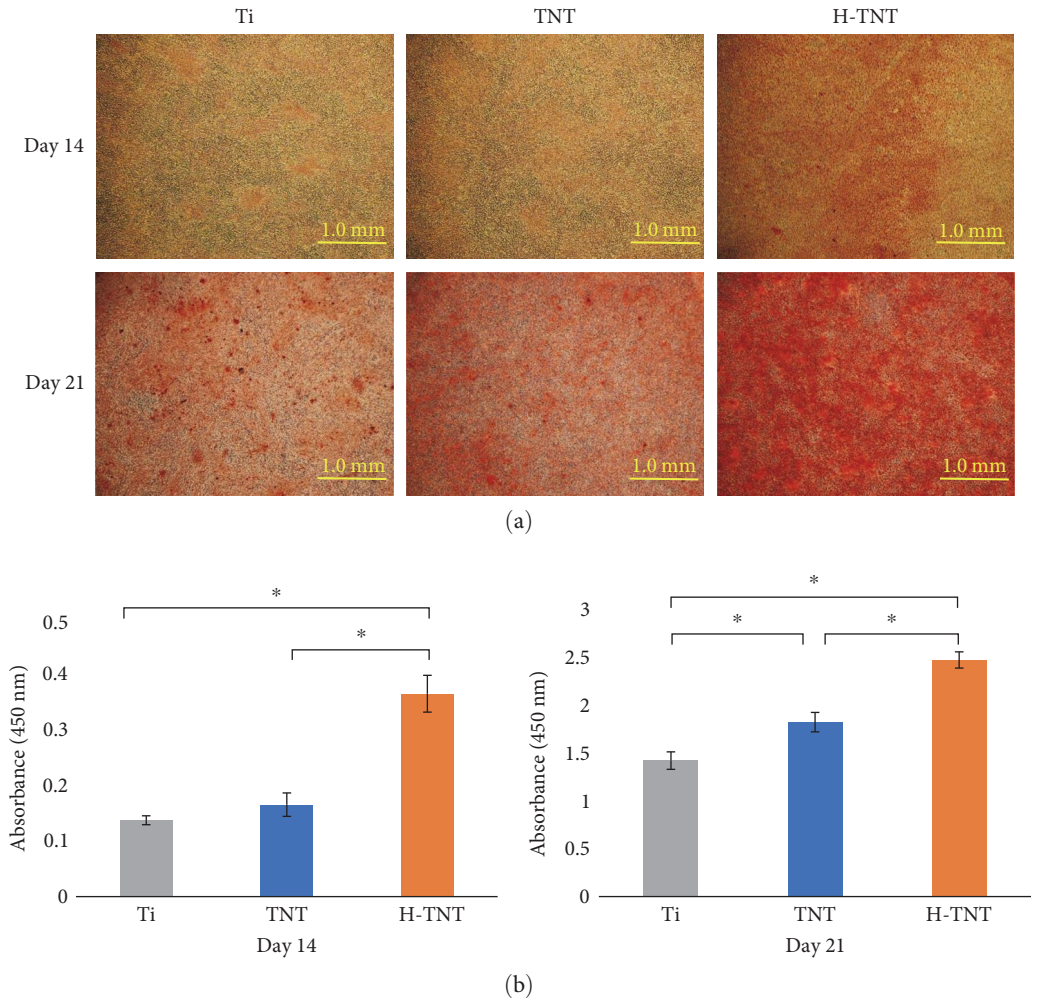

Figure 11: (a) Extracellular matrix mineralization of MC3T3-E1 cells after osteogenic induction for 14 and 21 days; (b) sample absorbance after the addition of 10% cetyl pyridinium chloride solution. $^*p < 0.05$. Abbreviations: H-TNT, hydrogenated TiO_2 nanotubes; Ti, pure titanium; TNT, air-annealed TiO_2 nanotubes.

Compared to the Ti and TNT samples, the MC3T3-E1 cells cocultured with H-TNT had an elongated, spindle-shaped morphology, which reportedly enhances osteoblast differentiation [39] and cell–cell communication, attributes that are critical for coordinating cell behavior [40]. A previous study demonstrated that nanotube topography supports cell stretching and differentiation [41]. Thus, the elongated shape can promote the osteogenic differentiation of MC3T3-E1 cells, which was confirmed by the ALP activity results in this study.

Cell adhesion and spread may affect their proliferation and differentiation [42, 43]. Our results (Figures 8 and 9) indicate that the H-TNT MCM has great potential for improving MC3T3-E1 cell adhesion, proliferation, and spread. This may be ascribed to the M2-type polarization of macrophages on H-TNT surface and anti-inflammatory cytokines and growth factors secreted by them. Specifically, ARG, IL-4, and IL-10 promote M2-type macrophage polarization and are involved in wound healing. M2-type macrophages secrete growth factors and chemokines related to bone healing and promote the migration and differentiation of osteoblasts, bone marrow mesenchymal stem cells, and vascular epithelial cells [10, 44]. Collectively, these factors may have enhanced MC3T3-E1 cell adhesion and proliferation observed in this study.

ALP analysis (Figure 10) suggests that the H-TNT MCM improves osteoinductivity. ALP is a hydrolase that is primarily involved in the hydrolysis of pyrophosphate in the early stages of osteogenesis, accelerating the formation of new bonds. It is also an important indicator of early osteocyte osteogenesis [45]. As observed in our study, the higher ALP activity and osteogenic gene expression induced by the H-TNT MCM significantly increased the mineralization of MC3T3-E1 cells.

The H-TNT samples showed an enhanced expression of osteogenesis-related genes, such as those encoding ALP, BMP-2, Runx-2, COL-1, and OPN [46]. BMP-2 is a key regulator of bone formation and promotes osteogenic differentiation and regeneration [47]. Furthermore, BMP-2 induces Runx-2 gene expression and promotes osteogenic differentiation [48], suggesting that the two proteins work together to facilitate the osteogenic differentiation of MC3T3-E1 cells. Moreover, COL-1 forms a scaffold for

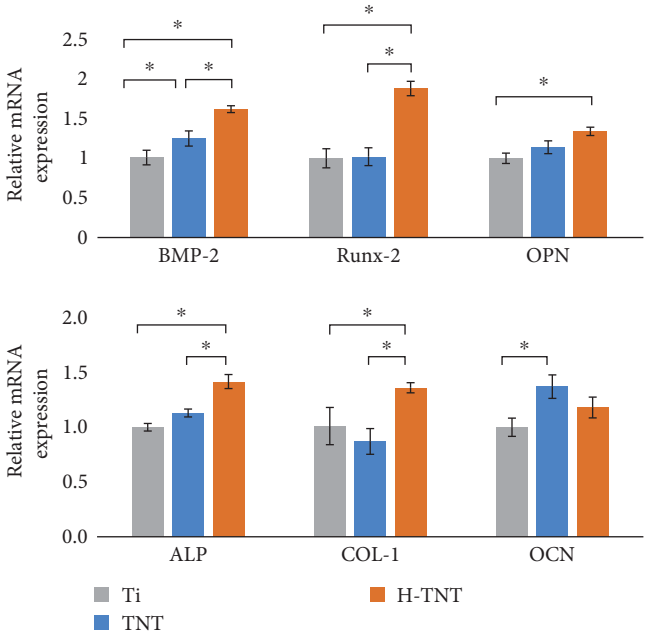

Figure 12: RT-PCR detection of osteogenic-related gene expression in MC3T3-E1 cells after a 3-day incubation with MCM. $^*p < 0.05$. Abbreviations: ALP, alkaline phosphatase; BMP-2, bone morphogenetic protein 2; COL-1, collagen type 1; H-TNT, hydrogenated TiO_2 nanotubes; MCM, macrophage-conditioned media; OCN, osteocalcin; OPN, osteopontin; Ti, pure titanium; TNT, air-annealed TiO_2 nanotubes.

calcium salt deposition to promote extracellular matrix mineralization in osteoblasts. The high COL-1 mRNA expression in the H-TNT sample may be attributed to the downregulated expression of inflammatory cytokines and promotion of extracellular matrix mineralization of MC3T3-E1 cells.

OPN is a glycosylated protein closely related to bone formation and development [49]. It is also a potential immunomodulatory factor that can exert proinflammatory effects [50] and inhibit mineralization through potential phosphorylation sites [51]. However, a recent report showed that macrophages from OPN-deficient mice mount a heightened inflammatory response, suggesting that OPN exerts anti-inflammatory effects [52]. Another research group reported that OPN acts as a mineralization promoter in collagen fibers [53]. In this study, the mRNA expression levels of OPN were higher in the H-TNT sample than in the Ti sample. Considering the heterogeneous and complex effects of OPN, we hypothesized that it balances the pro- and anti-inflammatory effects in bone reconstruction, which in turn facilitate the osteogenic differentiation of MC3T3-E1 cells. Both M1 and M2 macrophages are vital for immune response [54], and the transition of macrophages from M1 to M2 favors bone regeneration and repair [55].

Collectively, the results of this study demonstrate that H-TNT promotes osteoblast proliferation, adhesion, and differentiation potential by modulating the immune balance. However, their performance requires further investigation through in vivo testing.

5. Conclusions

H-TNT prepared by anodic oxidation and hydrogenation induced M2-type macrophage polarization and further promoted MC3T3-E1 cell adhesion, proliferation, and osteogenic differentiation. These materials are promising candidates for bone implants because they activate macrophages to produce a favorable osteoimmunomodulatory microenvironment.

Data Availability

The data used to support the findings of this study are included in the article. Further data or information are available from the corresponding author upon request.

Conflicts of Interest

The authors declare that they have no conflict of interests.

Authors' Contributions

Xu Cao and Ran Lu contributed equally to this work.

Acknowledgments

The authors gratefully acknowledge financial support from the National Natural Science Foundation of China (grant nos. 81873722 and 81570999).

Supplementary Materials

Figure S1: more cell samples of iNOS and ARG at 24 hr. Figure S2: more cell samples of CD80 and CD163 at 24 hr. Figure S3: more cell samples of CD80 and CD163 at 48 hr. Figure S4: quantitative analysis of fluorescent staining of iNOS and ARG at 24 hr. Figure S5: quantitative analysis of fluorescent staining of iNOS and ARG at 48 hr. Figure S6: quantitative analysis of fluorescent staining of CD80 and CD163 at 24 hr. Figure S7: quantitative analysis of fluorescent staining of CD80 and CD163 at 48 hr. (*Supplementary Materials*)

References

[1] M. L. Novak and T. J. Koh, "Macrophage phenotypes during tissue repair," *Journal of Leukocyte Biology*, vol. 93, no. 6, pp. 875–881, 2013.

[2] Z. Chen, A. Bachhuka, F. Wei et al., "Nanotopography-based strategy for the precise manipulation of osteoimmunomodulation in bone regeneration," *Nanoscale*, vol. 9, no. 46, pp. 18129–18152, 2017.

[3] E. M. O'Brien, G. E. Risser, and K. L. Spiller, "Sequential drug delivery to modulate macrophage behavior and enhance implant integration," *Advanced Drug Delivery Reviews*, vol. 149–150, pp. 85–94, 2019.

[4] F. Taraballi, B. Corradetti, S. Minardi et al., "Biomimetic collagenous scaffold to tune inflammation by targeting macrophages," *Journal of Tissue Engineering*, vol. 7, 2016.

[5] Z. Yuan, X. Zhu, Y. Li, P. Yan, and H. Jiang, "Influence of iRoot SP and mineral trioxide aggregate on the activation and polarization of macrophages induced by lipopolysaccharide," *BMC Oral Health*, vol. 18, Article ID 56, 2018.

[6] A. Chaudhuri, "Regulation of macrophage polarization by RON receptor tyrosine kinase signaling," *Frontiers in Immunology*, vol. 5, Article ID 546, 2014.

[7] A. Mantovani, A. Sica, S. Sozzani, P. Allavena, A. Vecchi, and M. Locati, "The chemokine system in diverse forms of macrophage activation and polarization," *Trends in Immunology*, vol. 25, no. 12, pp. 677–686, 2004.

[8] C. E. Witherel, D. Abebayehu, T. H. Barker, and K. L. Spiller, "Macrophage and fibroblast interactions in biomaterial-mediated fibrosis," *Advanced Healthcare Materials*, vol. 8, no. 4, Article ID e1801451, 2019.

[9] D. M. Mosser and J. P. Edwards, "Exploring the full spectrum of macrophage activation," *Nature Reviews Immunology*, vol. 8, pp. 958–969, 2008.

[10] J. Wang, S. Qian, X. Liu et al., "M2 macrophages contribute to osteogenesis and angiogenesis on nanotubular TiO_2 surfaces," *Journal of Materials Chemistry B*, vol. 5, no. 18, pp. 3364–3376, 2017.

[11] H. Kang, S. Kim, D. S. H. Wong et al., "Remote manipulation of ligand nano-oscillations regulates adhesion and polarization of macrophages in vivo," *Nano Letters*, vol. 17, no. 10, pp. 6415–6427, 2017.

[12] B. Li, Y. Hu, Y. Zhao et al., "Curcumin attenuates titanium particle-induced inflammation by regulating macrophage polarization in vitro and in vivo," *Frontiers in Immunology*, vol. 8, Article ID 55, 2017.

[13] K. M. Hotchkiss, G. B. Reddy, S. L. Hyzy, Z. Schwartz, B. D. Boyan, and R. Olivares-Navarrete, "Titanium surface characteristics, including topography and wettability, alter macrophage activation," *Acta Biomaterialia*, vol. 31, pp. 425–434, 2016.

[14] L. Dong, L. Li, Y. Song et al., "MSC-derived immunomodulatory extracellular matrix functionalized electrospun fibers for mitigating foreign-body reaction and tendon adhesion," *Acta Biomaterialia*, vol. 133, pp. 280–296, 2021.

[15] X. Yin, Y. Li, C. Yang et al., "Alginate/chitosan multilayer films coated on IL-4-loaded TiO_2 nanotubes for modulation of macrophage phenotype," *International Journal of Biological Macromolecules*, vol. 132, pp. 495–505, 2019.

[16] X. Yin, C. Yang, Z. Wang et al., "Alginate/chitosan modified immunomodulatory titanium implants for promoting osteogenesis in vitro and in vivo," *Materials Science and Engineering: C*, vol. 124, Article ID 112087, 2021.

[17] G. Tian, S. Jiang, J. Li et al., "Cell-free decellularized cartilage extracellular matrix scaffolds combined with interleukin 4 promote osteochondral repair through immunomodulatory macrophages: in vitro and in vivo preclinical study," *Acta Biomaterialia*, vol. 127, pp. 131–145, 2021.

[18] D. Karazisis, L. Rasmusson, S. Petronis et al., "The effects of controlled nanotopography, machined topography and their combination on molecular activities, bone formation and biomechanical stability during osseointegration," *Acta Biomaterialia*, vol. 136, pp. 279–290, 2021.

[19] D. Karazisis, S. Petronis, H. Agheli et al., "The influence of controlled surface nanotopography on the early biological events of osseointegration," *Acta Biomaterialia*, vol. 53, pp. 559–571, 2017.

[20] W. L. Lü, N. Wang, P. Gao, C. Y. Li, H. S. Zhao, and Z. T. Zhang, "Effects of anodic titanium dioxide nanotubes of different diameters on macrophage secretion and expression of cytokines and chemokines," *Cell Proliferation*, vol. 48, no. 1, pp. 95–104, 2015.

[21] Q. Wang, P. Zhou, S. Liu et al., "Multi-scale surface treatments of titanium implants for rapid osseointegration: a review," *Nanomaterials*, vol. 10, no. 6, Article ID 1244, 2020.

[22] L. Zhao, L. Liu, Z. Wu, Y. Zhang, and P. K. Chu, "Effects of micropitted/nanotubular titania topographies on bone mesenchymal stem cell osteogenic differentiation," *Biomaterials*, vol. 33, no. 9, pp. 2629–2641, 2012.

[23] K. S. Brammer, S. Oh, C. J. Cobb, L. M. Bjursten, H. van der Heyde, and S. Jin, "Improved bone-forming functionality on diameter-controlled TiO_2 nanotube surface," *Acta Biomaterialia*, vol. 5, no. 8, pp. 3215–3223, 2009.

[24] R. Lu, C. Wang, X. Wang et al., "Effects of hydrogenated TiO_2 nanotube arrays on protein adsorption and compatibility with osteoblast-like cells," *International Journal of Nanomedicine*, vol. 13, pp. 2037–2049, 2018.

[25] S. Gao, R. Lu, X. Wang et al., "Immune response of macrophages on super-hydrophilic TiO_2 nanotube arrays," *Journal of Biomaterials Applications*, vol. 34, no. 9, pp. 1239–1253, 2020.

[26] J. Wang, F. Meng, W. Song et al., "Nanostructured titanium regulates osseointegration via influencing macrophage polarization in the osteogenic environment," *International Journal of Nanomedicine*, vol. 13, pp. 4029–4043, 2018.

[27] N. Liu, V. Haublein, X. Zhou et al., "Black" TiO_2 nanotubes formed by high-energy proton implantation show noble-metal-*co*-catalyst free photocatalytic H_2-evolution," *Nano Letters*, vol. 15, no. 10, pp. 6815–6820, 2015.

[28] T. U. Luu, S. C. Gott, B. W. K. Woo, M. P. Rao, and W. F. Liu, "Micro- and nanopatterned topographical cues for regulating macrophage cell shape and phenotype," *ACS Applied Materials & Interfaces*, vol. 7, no. 51, pp. 28665–28672, 2015.

[29] A. K. Refai, M. Textor, D. M. Brunette, and J. D. Waterfield, "Effect of titanium surface topography on macrophage activation and secretion of proinflammatory cytokines and chemokines," *Journal of Biomedical Materials Research Part A*, vol. 70A, no. 2, pp. 194–205, 2004.

[30] R. J. Miron and D. D. Bosshardt, "OsteoMacs: key players around bone biomaterials," *Biomaterials*, vol. 82, pp. 1–19, 2016.

[31] L. Bai, Y. Yang, J. Mendhi et al., "The effects of TiO_2 nanotube arrays with different diameters on macrophage/endothelial cell response and ex vivo hemocompatibility," *Journal of Materials Chemistry B*, vol. 6, no. 39, pp. 6322–6333, 2018.

[32] K. Gulati, S. M. Hamlet, and S. Ivanovski, "Tailoring the immuno-responsiveness of anodized nano-engineered titanium implants," *Journal of Materials Chemistry B*, vol. 6, no. 18, pp. 2677–2689, 2018.

[33] K. M. Hotchkiss, N. M. Clark, and R. Olivares-Navarrete, "Macrophage response to hydrophilic biomaterials regulates MSC recruitment and T-helper cell populations," *Biomaterials*, vol. 182, pp. 202–215, 2018.

[34] K. M. Hotchkiss, K. T. Sowers, and R. Olivares-Navarrete, "Novel in vitro comparative model of osteogenic and inflammatory cell response to dental implants," *Dental Materials*, vol. 35, no. 1, pp. 176–184, 2019.

[35] K. Gulati, H.-J. Moon, T. Li, P. T. Sudheesh Kumar, and S. Ivanovski, "Titania nanopores with dual micro-/nano-topography for selective cellular bioactivity," *Materials Science and Engineering: C*, vol. 91, pp. 624–630, 2018.

[36] Z. Hu, C. Ma, X. Rong, S. Zou, and X. Liu, "Immunomodulatory ECM-like microspheres for accelerated bone regeneration

in diabetes mellitus," *ACS Applied Materials & Interfaces*, vol. 10, no. 3, pp. 2377–2390, 2018.

[37] L. Gao, M. Li, L. Yin et al., "Dual-inflammatory cytokines on TiO_2 nanotube-coated surfaces used for regulating macrophage polarization in bone implants," *Journal of Biomedical Materials Research Part A*, vol. 106, no. 7, pp. 1878–1886, 2018.

[38] W.-Q. Yu, X.-Q. Jiang, F.-Q. Zhang, and L. Xu, "The effect of anatase TiO_2 nanotube layers on MC3T3-E1 preosteoblast adhesion, proliferation, and differentiation," *Journal of Biomedical Materials Research Part A*, vol. 94A, no. 4, pp. 1012–1022, 2010.

[39] D. Li, Y. Li, A. Shrestha et al., "Effects of programmed local delivery from a micro/nano-hierarchical surface on titanium implant on infection clearance and osteogenic induction in an infected bone defect," *Advanced Healthcare Materials*, vol. 8, no. 11, Article ID e1900002, 2019.

[40] R. Civitelli, "Cell-cell communication in the osteoblast/osteocyte lineage," *Archives of Biochemistry and Biophysics*, vol. 473, no. 2, pp. 188–192, 2008.

[41] N. Wang, H. Li, J. Wang, S. Chen, Y. Ma, and Z. Zhang, "Study on the anticorrosion, biocompatibility, and osteoinductivity of tantalum decorated with tantalum oxide nanotube array films," *ACS Applied Materials & Interfaces*, vol. 4, no. 9, pp. 4516–4523, 2012.

[42] M. Cheng, Y. Qiao, Q. Wang et al., "Calcium plasma implanted titanium surface with hierarchical microstructure for improving the bone formation," *ACS Applied Materials & Interfaces*, vol. 7, no. 23, pp. 13053–13061, 2015.

[43] P. Jiang, J. Liang, R. Song et al., "Effect of octacalcium-phosphate-modified micro/nanostructured titania surfaces on osteoblast response," *ACS Applied Materials & Interfaces*, vol. 7, no. 26, pp. 14384–14396, 2015.

[44] S. J. Sun, W. Q. Yu, Y. L. Zhang, X. Q. Jiang, and F. Q. Zhang, "Effects of TiO_2 nanotube layers on RAW 264.7 macrophage behaviour and bone morphogenetic protein-2 expression," *Cell Proliferation*, vol. 46, no. 6, pp. 685–694, 2013.

[45] H. Orimo and T. Shimada, "The role of tissue-nonspecific alkaline phosphatase in the phosphate-induced activation of alkaline phosphatase and mineralization in SaOS-2 human osteoblast-like cells," *Molecular and Cellular Biochemistry*, vol. 315, pp. 51–60, 2008.

[46] Y. He, C. Mu, X. Shen et al., "Peptide LL-37 coating on microstructured titanium implants to facilitate bone formation in vivo via mesenchymal stem cell recruitment," *Acta Biomaterialia*, vol. 80, pp. 412–424, 2018.

[47] C.-Y. Lin, Y.-H. Chang, K.-J. Lin et al., "The healing of critical-sized femoral segmental bone defects in rabbits using baculovirus-engineered mesenchymal stem cells," *Biomaterials*, vol. 31, no. 12, pp. 3222–3230, 2010.

[48] M.-H. Lee, Y.-J. Kim, H.-J. Kim et al., "BMP-2-induced Runx2 expression is mediated by Dlx5, and TGF-β1 opposes the BMP-2-induced osteoblast differentiation by suppression of Dlx5 expression," *Journal of Biological Chemistry*, vol. 278, no. 36, pp. 34387–34394, 2003.

[49] A. Singh, G. Gill, H. Kaur, M. Amhmed, and H. Jakhu, "Role of osteopontin in bone remodeling and orthodontic tooth movement: a review," *Progress in Orthodontics*, vol. 19, Article ID 18, 2018.

[50] M. A. Icer and M. Gezmen-Karadag, "The multiple functions and mechanisms of osteopontin," *Clinical Biochemistry*, vol. 59, pp. 17–24, 2018.

[51] R. Sapir-Koren and G. Livshits, "Bone mineralization and regulation of phosphate homeostasis," *IBMS BoneKEy*, vol. 8, no. 6, pp. 286–300, 2011.

[52] H. Yang, X. Ye, X. Zhang, X. Li, Q. Fu, and Z. Tang, "Intracellular osteopontin negatively regulates toll-like receptor 4-mediated inflammatory response via regulating GSK3β and 4EBP1 phosphorylation," *Cytokine*, vol. 108, pp. 89–95, 2018.

[53] D. E. Rodriguez, T. Thula-Mata, E. J. Toro et al., "Multifunctional role of osteopontin in directing intrafibrillar mineralization of collagen and activation of osteoclasts," *Acta Biomaterialia*, vol. 10, no. 1, pp. 494–507, 2014.

[54] K. E. Martin and A. J. García, "Macrophage phenotypes in tissue repair and the foreign body response: implications for biomaterial-based regenerative medicine strategies," *Acta Biomaterialia*, vol. 133, pp. 4–16, 2021.

[55] Z. Chen, T. Klein, R. Z. Murray et al., "Osteoimmunomodulation for the development of advanced bone biomaterials," *Materials Today*, vol. 19, no. 6, pp. 304–321, 2016.